ORGANIC CHEMISTRY FRONTIERS

RESEARCH ARTICLE

View Article Online
View Journal

Cite this: DOI: 10.1039/d5qo01401h

[2.2]Paracyclophane–dicyanorhodanine conjugates as planar chiral molecular photoswitches

Parag Das, Cole D. Stearns, Ion Ghiviriga, Łukasz Dobrzycki and Ronald K. Castellano *

(Chir)optical molecular photoswitches have garnered significant attention for their applications in asymmetric synthesis, supramolecular chemistry, and the materials sciences. The planar chirality and associated photophysical and chiroptical properties of [2.2]paracyclophane ([2.2]pCp) derivatives have been long appreciated. Even so, chiral photoswitches incorporating the [2.2]pCp framework remain largely unexplored. Dicyanorhodanine (RCN), conjugated with oligothiophenes and pyrroles, has been recently shown as a highly competent photoisomerizable scaffold. The current work introduces a novel photoswitch system combining an electron-rich [2.2]pCp moiety with an electron-deficient RCN unit, as a planar chiral "push–pull" architecture. Single crystal X-ray study reveals the *Z* configuration for the as-synthesized RCN–pCp conjugate; upon visible light irradiation well-controlled and reversible *Z*/*E* photoisomerization is observed to achieve a photostationary state distribution (PSD) up to 40/60 (*Z*/*E*). The model chromophores exhibit negative solvatochromism across solvents of different polarity. Engineering the "push–pull" electronic structure by introducing an electron-donating methoxy group influences the photophysical properties and the photo- and thermal isomerization behavior. An enantioenriched planar chiral photoswitch based on the RCN–pCp scaffold is also introduced, that displays a reversible chiroptical response as evaluated by circular dichroism (CD) spectroscopy as a consequence of *Z*/*E* photoisomerization. Ground-state (DFT) and excited-state (TD-DFT) calculations correlate well with the experimental geometries and the spectral (UV–vis and CD) characteristics, respectively. We are optimistic that the reported planar chiral [2.2]pCp-based photoswitches will facilitate the design of next-generation photoresponsive organic functional materials.

Received 9th October 2025,
Accepted 27th October 2025
DOI: 10.1039/d5qo01401h
rsc.li/frontiers-organic

Introduction

Chiral molecular photoswitches are a dynamic class of stimuli-responsive chromophores availing two or more isomeric states with distinct chiroptical properties.[1–3] Reversibly interchangeable chiral optical signals, such as electronic circular dichroism (ECD) and circularly polarized luminescence (CPL), offer promising applications across many scientific disciplines including chiral sensing,[4] asymmetric synthesis,[5] liquid-crystalline materials,[6,7] information storage,[8] supramolecular chemistry,[9–11] and so on. "Chiroptical photoswitches" have been efficiently designed by integrating chiral elements with photoresponsive components, to reversibly control the axial, planar, or helical chirality of the systems using a non-invasive stimulus, light, with a high spatiotemporal resolution.[12–14] Popular small-molecule photoswitchable scaffolds like hemithioindigoes,[15,16] hydrazones,[17,18] and arylazopyrazoles[19,20] have shown versatile applications in materials science, molecular machines, and supramolecular chemistry.[21–23] Importantly, in recent years, developing chiral photoswitches has become an intriguing pursuit through careful design based on photoisomerizable units like hemi(phospho) indigos,[24,25] diarylethenes,[26,27] overcrowded alkenes,[28,29] azobenzenes,[30,31] *etc*. Dube and co-workers reported axially chiral hemiindigo photoswitches with reversible chiroptical signals (Fig. 1a).[24] A diarylethene-derived chiral photoswitch was designed by Ubukata, *et al.*, showing helicity interconversion between a binaphthyl state and a helicenoid skeleton (Fig. 1b).[27]

[2.2]Paracyclophane ([2.2]pCp)[32,33] is a compact, tunable, and practical three-dimensional (3D) scaffold with well described physicochemical and stereoelectronic properties owing to its "transannular through-space" and "through-bond" interactions.[34,35] Functionalized [2.2]pCp architectures show

Department of Chemistry, University of Florida, PO Box 117200, Gainesville, Florida 32611, USA. E-mail: castellano@chem.ufl.edu

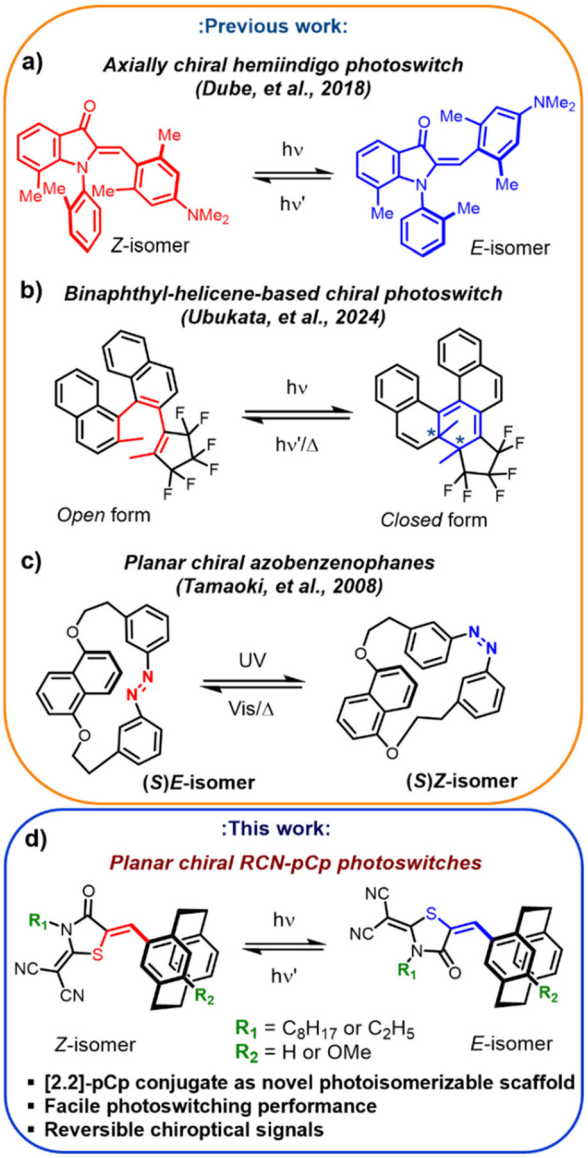

Fig. 1 Previous reports: (a) axially chiral hemiindigo photoswitches[24] by Dube, *et al.*, (b) a binaphthyl-helicene-based chiral photoswitch[27] by Ubukata, *et al.*, and (c) planar chiral azobenzenophanes by Tamaoki, *et al.*[51] (d) This work introduces a planar chiral [2.2]pCp structure conjugated with the RCN unit as an efficient photoisomerizable scaffold.

attractive features in supramolecular self-assembly,[36,37] fluorescent dyes,[38] and organic functional materials.[39] [2.2]pCps with specific substitution patterns exhibit planar chirality due to the hindered rotation of their aryl moieties,[40] and possess attractive spectroscopic properties,[41] leading to broad optoelectronic applications.[42–44]

Although structure–property relationships of [2.2]pCp derivatives have been widely reported,[45] controlling their chiroptical properties reversibly using an external stimulus has been scarcely studied.[46,47] Noteworthy examples in this context include macrocyclic oligoazobenzenophanes[48] and perylene bisimide (PBI) cyclophane[49] derivatives, the photophysical properties of which can be modulated through the *trans*/*cis* photoisomerization of the azobenzene moiety. Moreover, the induced planar chirality of twisted azo dopants has attracted considerable interest in the field of cholesteric liquid crystals (LC);[50] one example includes a planar chiral azobenzenophane developed by Tamaoki, *et al.*, achieving phototunable reflection colors in nematic liquid crystals (Fig. 1c).[51]

Dicyanorhodanine, abbreviated as RCN,[52] is an electron-deficient heterocycle, and an integral component of donor–acceptor-type organic photovoltaic (OPV) materials.[53] Although the electron-acceptor RCN unit is more popular for constructing π-conjugated oligomeric organic materials, our group has showcased its proficiency in designing photoisomerizable small-molecules.[54,55] RCN-functionalized oligothiophenes, for example, can undergo *Z*/*E* photoisomerization in solution;[54,56] in the context of thin films, significant changes in optoelectronic properties attributed to the different solid-state morphologies of the *Z* and *E* isomers results.[57] More recently, we have introduced RCN–pyrrole conjugates as quantitative photoswitches in solution and thin films, and highlighted the role of hydrogen-bonding interactions crucial for their effective photoisomerization and isomeric bistability.[55]

Through-space charge transfer across the paracyclophane π-decks is facile, similar to a π-conjugated linker of the same length.[58,59] As a result, its electronic properties resemble a benzene excimer and provide electron-rich activity similar to thiophene.[60–62] Considering previously reported photoisomerization of RCN-functionalized (hetero)aromatic scaffolds, the electronic contribution of [2.2]pCp can be investigated in the context of small-molecule photoswitches when appended with the electron-deficient RCN unit. This molecular design would enable accessing a novel planar chiral "push–pull" type charge-transfer chromophore, suitable for *Z*/*E* photoisomerization. Moreover, [2.2]pCp-functionalized π-conjugated "push–pull" oligomers and polymers have been extensively studied for the development of organic nonlinear optical materials,[63–65] and the "push–pull" characteristic is highly advantageous also for improving photoisomerization efficiency.[66,67] Alongside tuning the optical properties of the RCN–pCp structures, reversibly controlling the chiral signals would be highly desirable and appealing for materials chemistry and optical cryptography.[68,69]

Herein, we report the design, synthesis, and *Z*/*E* photoisomerization behavior of planar chiral [2.2]pCp–RCN conjugates and have evaluated their phototunable (chir)optical properties (Fig. 1d). All the racemic and enantioenriched "as-synthesized" compounds feature the *Z* stereochemistry about the exocyclic olefin bond that conjugates the RCN to the chiral pCp unit, as confirmed from single crystal X-ray analysis and 2D-NMR spectroscopy. Well-controlled reversible *Z*/*E* photoisomerization is obtained for all three racemic model compounds using selective visible-light photoirradiation (λ_{irr} = 404, 454, and 523 nm). ^{1}H NMR studies show 57%–60% $Z \rightarrow E$ photoconversion, and near quantitative (92%–98%) $E \rightarrow Z$ photoreversion. The photophysical properties of the chromophores have been evaluated in different polarity solvents, and

a hypsochromic shift but well-behaved reversible photoisomerization has been observed in more polar ones. The introduction of an electron-donating methoxy group (–OMe) provides a stronger push–pull character and red-shifts the absorption profile, also leading to excellent photostability over ten photoswitching cycles. One prepared enantioenriched chiral pCp photoswitch shows a similar extent of photoisomerization to its racemic analog, and the chiroptical signal obtained for the pure *Z* isomer can be reversibly weakened and amplified using visible-light excitation. We believe these in-depth solution photoisomerization studies, accompanied by comprehensive theoretical investigations, of the planar chiral RCN–pCp scaffolds will pave the way for their usage as highly functional chiroptical materials in the future.

Results and discussion

Design and synthesis

Considering the planar chirality of the cyclophane scaffold, preparation of RCN–pCp photoswitches from racemic precursors provides four possible stereoisomers: (***R*****$_p$**)-***Z***, (***R*****$_p$**)-***E***, (***S*****$_p$**)-***Z***, and (***S*****$_p$**)-***E*** (Fig. 2). ***R*****$_p$** and ***S*****$_p$** enantiomers result from the planar chirality induced by mono-substitution of the RCN unit at the [2.2]pCp scaffold, while ***Z*** and ***E*** geometric isomers can be assigned based on the substituents at the exocyclic olefin bond. While the (***R*****$_p$** or ***S*****$_p$**) ***Z*** and (***R*****$_p$** or ***S*****$_p$**) ***E*** geometric photoisomers can be interconverted using selective wavelength irradiation, the parent chirality of each compound cannot be interchanged (*i.e.*, ***R*****$_p$** → ***S*****$_p$** or ***S*****$_p$** → ***R*****$_p$**).

We first synthesized three racemic model RCN–pCp compounds to evaluate the photoisomerization behavior of such planar chiral chromophores. Among them, compounds **(±)-1-*Z*** and **(±)-2-*Z*** represent the simplest RCN–pCp analogs, differing only in the length of the alkyl chain attached to the RCN unit. The presence of an octyl chain in compound **(±)-1-*Z*** enhances its solubility across a wide range of solvents. In contrast, compound **(±)-2-*Z***, containing a shorter ethyl group, has been primarily designed for crystallization purposes. RCN units **4** and **6** were synthesized using multi-component Knoevenagel condensation reactions,[56,70] and the racemic aldehyde **(±)-5** was obtained through Rieche formylation of the commercially available [2.2]pCp precursor (Schemes S1 and S2).[71] The aldehyde was subsequently condensed with the appropriate RCN units to afford the final photoswitches **(±)-1-*Z*** and **(±)-2-*Z*** (Schemes 1 and S1, S2).

In compound **(±)-3-*Z***, an electron-donating (EDG) methoxy (–OMe) group is installed at the *para*-position of the RCN unit to strengthen the "push–pull" character and influence the photochromism.[55] Aldehyde **(±)-9** was synthesized in three steps from **(±)-5**, using hydroxylation, methylation, and formylation reactions (Scheme S3).[72] A Knoevenagel condensation between **6** and **(±)-9** yields compound **(±)-3-*Z*** (Schemes 1 and S3). All the target RCN–pCp compounds were obtained in the *Z* configuration as the only detectable isomer from the synthesis. The *E* isomer was obtained post-irradiation as a *Z*/*E* mixture in solution and could be purified using silica column chromatography. Due to very similar R_f values of the *Z* and *E* isomers by Thin Layer Chromatography (TLC), only 94% *E* isomer could be obtained as a 94/6 (*E*/*Z*) mixture for compound **(±)-1** (Fig. S54) which was used for detailed structural characterization (*vide infra*).

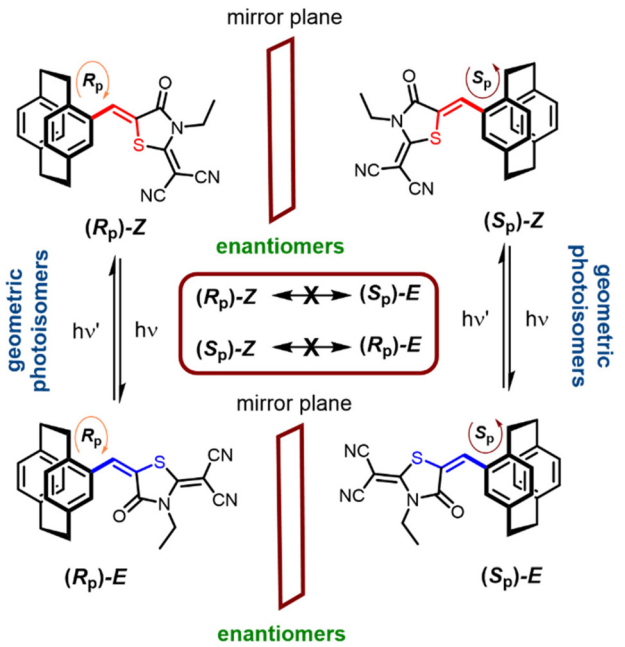

Fig. 2 Stereoisomerism of the RCN–pCp conjugates including ***R*****$_p$** and ***S*****$_p$** enantiomers, and ***Z*** and ***E*** configurational photoisomers.

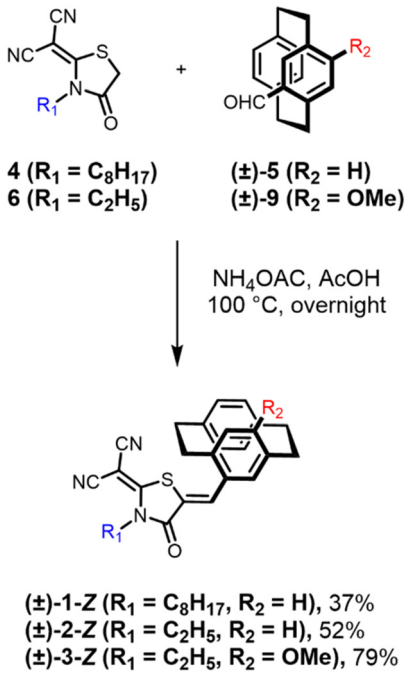

Scheme 1 Synthesis of racemic target molecules **(±)-1-*Z*–(±)-3-*Z***.

Full synthetic schemes and characterization details for the racemic target molecules **(±)-1–(±)-3** and related intermediates are provided in the SI (Schemes S1–S3 and Fig. S1–S10, S15–S24).

Stereochemical determination

The stereochemistry of the exocyclic olefin bond of the as-synthesized isomers was determined from single crystal X-ray analysis of compound **(±)-3-*Z*** (pages S77–S81). Interestingly, the structure is disordered and contains both the *Z* and *E* isomer sharing the same site due to possible co-crystallization (Fig. S98–S100). The as-synthesized isomer *Z* is the major component (Fig. S101) of the crystal with occupancy exceeding 95% and the remaining *ca.* 5% is the *E* isomer (Fig. S102) presumably formed upon photoirradiation during the crystallization process under laboratory conditions. In the crystal structure of **(±)-3-*Z***, the main component, *i.e.*, the *Z* isomer, adopts a slightly twisted geometry (Fig. 3a and b), with deviation from planarity defined by the dihedral angles S19–C18–C17–C1 (6.33°) and S1–C14–C24–C25 (−179.1°). The long-range packing of the major component of the crystal displays a head-to-tail slip-stack arrangement (Fig. 3c). The π-stacked head-to-tail dimers of two *Z* monomers present in the solid state might persist in solution, governed by weak association. We have observed minimal deshielding ($\Delta\delta$ = 0.04 ppm) of the olefinic and aromatic protons upon increasing the temperature (25 → 90 °C, in tetrachloroethane-d_2), still potentially consistent with π–π interactions (Fig. S76 and S77).

A comprehensive 2D-NMR spectroscopic investigation (in acetone-d_6) was performed using **(±)-1-*Z*** and **(±)-1-*E*** (94%) for additional structural confirmation of the *Z* and *E* isomers (Fig. S27–S48). Heteronuclear 2D correlation techniques like HSQC and HMBC, along with homonuclear 1D correlation spectroscopic studies such as NOESY and TOCSY, were applied for the full characterization of the isomers (Fig. S27). In-phase/antiphase gradient-selected heteronuclear single- and multiple-bond correlation (IPAP-gHSMBC) spectroscopy (Fig. S48) of **(±)-1-*Z*** and **(±)-1-*E*** (94%) indicates the three-bond heteronuclear coupling ($^{1,3}J$) between the RCN carbonyl carbon (C22) and the isomerizable olefin proton (H17) is larger for the *E* isomer ($^{1,3}J_{C22–H17}$ = 11.9 Hz) compared to the *Z* ($^{1,3}J_{C22–H17}$ = 6.05 Hz), which is in agreement with our previous reports for RCN–thiophene[54] and RCN–pyrrole systems.[55] ^{1}H NMR studies (in chloroform-*d*) reveal that the olefin proton (H17) attached to the isomerizable C=C bond is considerably deshielded for the *Z* isomer (δ = 8.01 ppm) compared to *E* (δ = 7.34 ppm), owing to its proximity to the electron-withdrawing carbonyl group of the RCN unit in the *Z* configuration (Fig. S3 and S4).

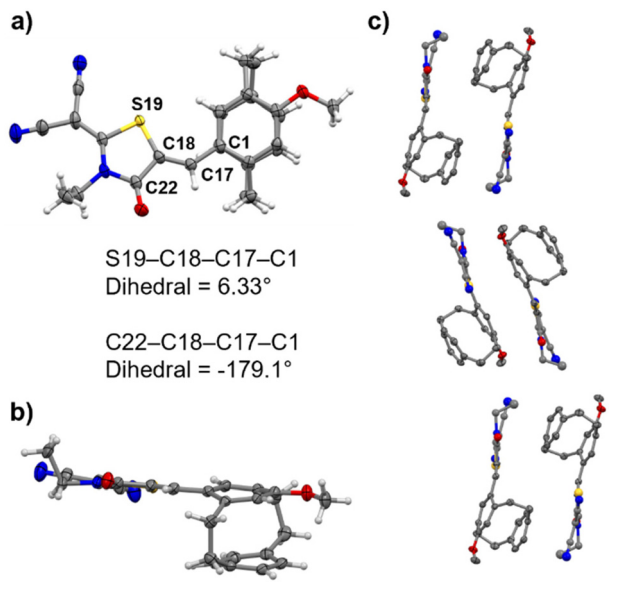

Fig. 3 Presentation of the major component of **(±)-3-*Z*** – isomer *Z*. (a) Thermal ellipsoid plot at 50% probability level, face-on view. (b) Edge-on view. (c) Long-range packing in the solid state (CCDC number: 2480804).

To gain further insight into the structural characteristics of the RCN–pCp compounds, we performed detailed ground-state (DFT) geometry optimization and energy calculations at the B3LYP/6-31+G(d) level of theory. To estimate the effect of solvent, supplemental calculations were performed using the IEFPCM solvent cavity reaction field.[73,74] Both the *Z* and *E* isomers can adopt two distinct conformations based on the position of the olefin proton (H17) with respect to its nearest bridge. The "conformer A" ($\mathbf{C_A}$) contains the olefin proton pointing towards the nearest ethylene bridge, whereas "conformer B" ($\mathbf{C_B}$) has the same proton pointing away from the bridged atoms. The $\mathbf{C_A}$ of the *Z* and *E* isomers is nearly planar (Fig. S89 and S91); however, the $\mathbf{C_B}$ adopts a highly twisted geometry (Fig. S90 and S92). The steric clash between the bridge protons of the top deck of the cyclophane unit and the sulfur atom (S19) of RCN in the *Z* isomer (and the carbonyl group of RCN in the *E* isomer) leads to distortion in $\mathbf{C_B}$, which is considerably reduced in $\mathbf{C_A}$. As a result, for compound **(±)-2**, **2-*Z*-$\mathbf{C_A}$** is thermodynamically most stable, and 5.47 kcal mol^{-1} (calculated in gas-phase) lower in energy than **2-*E*-$\mathbf{C_A}$** (Fig. S89). The twisted structures **2-*Z*-$\mathbf{C_B}$** and **2-*E*-$\mathbf{C_B}$** (Fig. S90) are 2.11 and 7.30 kcal mol^{-1} higher in energy than the most stable conformer (**2-*Z*-$\mathbf{C_A}$**), respectively. Solvent-corrected calculations (IEFPCM, chloroform) also present the **2-*Z*-$\mathbf{C_A}$** conformer as thermodynamically more stable than **2-*E*-$\mathbf{C_A}$** by 5.38 kcal mol^{-1} (Fig. S97). Similarly, for compound **(±)-3**, **3-*Z*-$\mathbf{C_A}$** is thermodynamically most stable, and 5.10 kcal mol^{-1} (calculated in gas-phase) lower in energy than **3-*E*-$\mathbf{C_A}$** (Fig. 4 and S91). This DFT analysis is well supported by experimental X-ray data as the single crystal of compound **(±)-3-*Z*** also confirms $\mathbf{C_A}$ as the "as-synthesized" conformer.

NMR photoisomerization studies

The photoisomerization reactions of the RCN–pCp conjugates were monitored by ^{1}H NMR spectroscopy (15 mM, chloroform-*d*) using selective irradiation sources (Fig. S53). For compound **(±)-1**, *Z* → *E* isomerization (Fig. S55) was evaluated at 404 nm excitation, and the photostationary state distribution (PSD) was observed as 43/57 (**(±)-1-*Z*/(±)-1-*E***). The metastable *E* isomer can revert to the *Z* isomer upon 454 nm irradiation with a photostationary state (PSS) ratio of 92/8 (**(±)-1-*Z*/(±)-1-*E***).

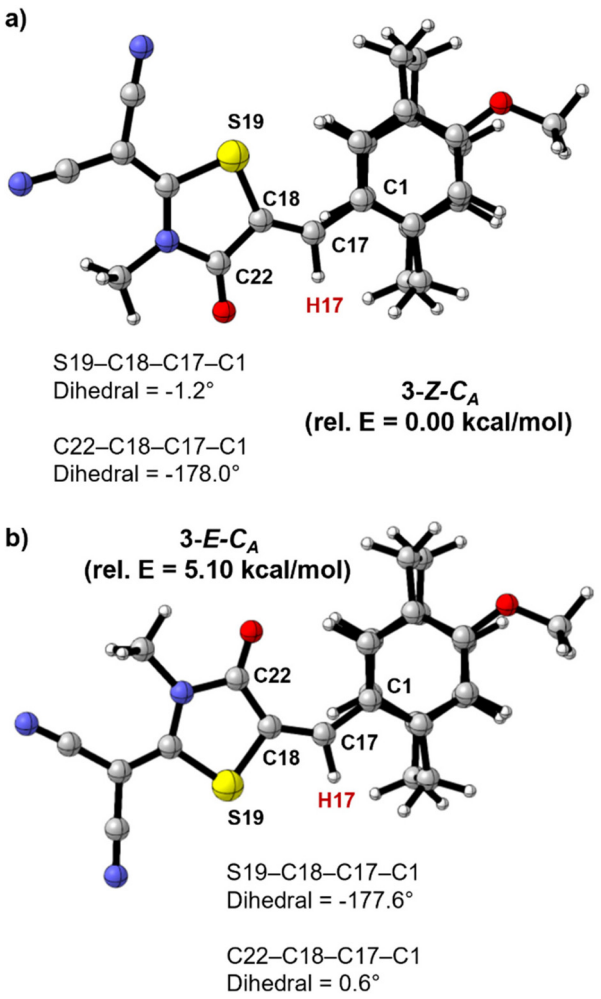

Fig. 4 Optimized lowest energy conformers (DFT, B3LYP/6-31+G(d)) of (a) **(±)-3-*Z*** (face-on view) and (b) **(±)-3-*E*** (face-on view), as modeled in conformation A (C_A) where the olefin proton (H17, marked in red) is pointing towards the bridge. The relative energy (rel. *E*) of the conformers has been denoted in parentheses.

Using a 371 nm UV lamp (Fig. S56), a similar extent of $Z \rightarrow E$ isomerization was obtained (**(±)-1-*Z*/(±)-1-*E*** = 42/58). The photoisomerization behavior of compound **(±)-1** was also studied in different polarity solvents (toluene and acetonitrile). In non-polar toluene-d_8, PSDs (**(±)-1-*Z*/(±)-1-*E***) of 47/53 and 95/5 were obtained for $Z \rightarrow E$ (λ_{irr} = 404 nm) and of $E \rightarrow Z$ isomerization (λ_{irr} = 454 nm), respectively (Fig. S57). In a polar solvent like acetonitrile-d_3, selective excitation at 404 nm ($Z \rightarrow E$ isomerization) and 454 nm ($E \rightarrow Z$ isomerization) yields PSDs (**(±)-1-*Z*/(±)-1-*E***) of 43/57 and 87/13, respectively (Fig. S58).

Although solvent polarity can dictate different mechanistic photo-induced pathways opposed to double-bond isomerization,[75] excitingly, only well-controlled reversible *Z*/*E* photoisomerization was observed in all three solvents (toluene, chloroform, and acetonitrile) for this RCN–pCp conjugate **(±)-1**. The subtle differences noted in the PSDs in different solvents suggest a negligible influence of solvation on the photoisomerization process.

For compound **(±)-2**, $Z \rightarrow E$ photoisomerization was affected using 404 nm (Fig. S59) and 371 nm (Fig. S60) LEDs to yield PSS ratios (**(±)-2-*Z*/(±)-2-*E***) of 43/57 and 42/58, respectively. A 92/8 (**(±)-2-*Z*/(±)-2-*E***) mixture was obtained upon $E \rightarrow Z$ photoisomerization with 454 nm excitation (Fig. S59 and Table 1). The very similar extent of photoisomerization for compounds **(±)-1-*Z*** and **(±)-2-*Z*** reveals that the RCN alkyl chain has no effect on the isomerization behavior.

Compound **(±)-3** undergoes 60% $Z \rightarrow E$ conversion (*Z*/*E* = 40/60) upon 404 nm photoirradiation and near quantitative $E \rightarrow Z$ photoisomerization (*Z*/*E* = 98/2) with 523 nm excitation (Fig. 5, S61 and Table 1). $Z \rightarrow E$ photoisomerization was also tested using 371 nm and 454 nm LEDs, resulting in PSDs (**(±)-3-*Z*/(±)-3-*E***) of 47/53 and 56/44 (Fig. S62). Although the inclusion of the –OMe group promotes a red-shifted absorption profile (*vide infra*) for compound **(±)-3-*Z***, the extent of $Z \rightarrow E$ photoisomerization (60%) does not differ significantly from **(±)-2-*Z*** (57%) due to a similar difference in absorption maxima ($\Delta\lambda_{max}$ = 18 nm) between the *Z* and *E* isomers (Table 1). Interestingly, the rate of $Z \rightarrow E$ photoisomerization (15 mM, chloroform-*d*) is slightly faster for compound **(±)-3-*Z*** (k = (8.16 ± 0.26) × 10^{-4} s^{-1}) *versus* **(±)-2-*Z*** (k = (7.00 ± 0.25) × 10^{-4} s^{-1}), presumably given the electron-donating effect of the methoxy substituent (Fig. S64–S66 and Table S1).[76,77]

UV–Vis photoisomerization studies

The photophysical properties of the racemic RCN–pCp conjugates were assessed by UV-vis spectroscopy. The absorption

Table 1 DFT-simulated and solution absorption and photoisomerization studies of model compounds **(±)-2** and **(±)-3**

	Gas-phase DFT studies[a]				Solution studies in chloroform		
	Relative energy (kcal mol^{-1})		Absorption maximum (nm)		Absorption maximum[b] (nm)	*Z*/*E* composition (%/%) at the PSS[c]	
Model compounds	*Z*	*E*	*Z*	*E*	*Z*	$Z \rightarrow E$ (λ_{irr} in nm)	$E \rightarrow Z$ (λ_{irr} in nm)
(±)-2	0	5.47	357	375	416	43/57 (404)	92/8 (454)
(±)-3	0	5.10	371	389	450	40/60 (404)	98/2 (523)

[a] The calculated relative energies and absorption maxima are reported for the most stable conformer (C_A) in the *Z* and *E* states. [b] Only the *Z* isomer is reported, as independent studies of the pure *E* isomer could not be performed in solution. [c] For each sample, the PSS ratios have been reported based on three measurements (with an error of ±1%).

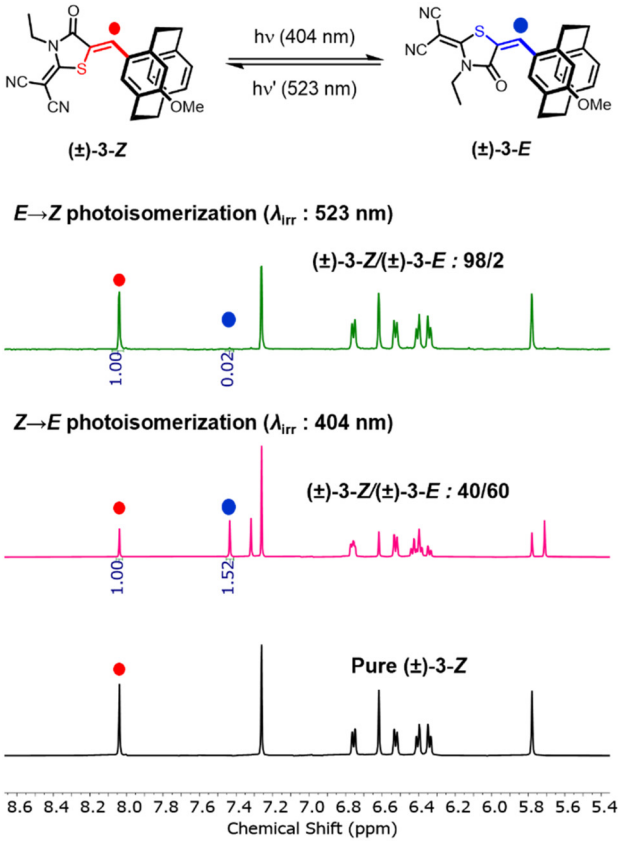

Fig. 5 Solution ^{1}H NMR (15 mM, $CDCl_3$) photoisomerization studies of compound **(±)-3-*Z***: pure *Z* isomer (bottom, black spectrum); PSS spectra obtained upon 404 nm irradiation (*Z* → *E* isomerization, pink spectrum) and 523 nm irradiation (*E* → *Z* isomerization, green spectrum).

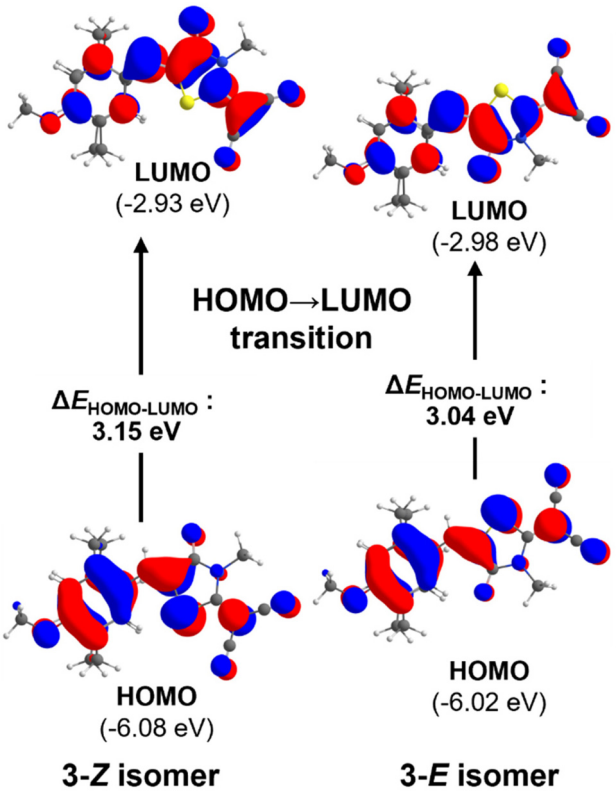

Fig. 6 Representations and energies of the frontier molecular orbitals of the **3-*Z*** and **3-*E*** isomers (in conformation A) showing the HOMO–LUMO transition.

profile of compound **(±)-1-*Z*** (20 μM, chloroform) features a primary absorption band at 416 nm (Fig. S78a), which can be classified as a π → π* intramolecular charge transfer (ITC) band,[52] along with secondary transition bands in the lower wavelength region (250–300 nm). While compound **(±)-2-*Z*** shows a very similar absorption profile (λ_{max} = 416 nm) to **(±)-1-*Z***, a 34 nm red-shift (λ_{max} = 450 nm) is observed for compound **(±)-3-*Z*** (Fig. 7a). As independent photophysical studies of pure *E* isomers could not be performed, we used time-dependent density functional theory (TD-DFT) to calculate the UV-vis profiles of the isomers using a range-separated hybrid functional (CAM-B3LYP) and double-ζ basis set (cc-pVDZ), which has proved adequate for RCN-functionalized donor–acceptor type scaffolds.[78] Detailed inspection of the frontier molecular orbitals (FMOs) of compounds **(±)-3-*Z*** (Tables S4, S5 and Fig. S95) and **(±)-3-*E*** (Tables S6, S7 and Fig. S96) suggest that the primary absorption band can be attributed to a HOMO–LUMO transition (Fig. 6), and the secondary absorption band corresponds to multiple π → π* transitions including HOMO−3–LUMO+2 (for the *Z* isomer) and HOMO−6–LUMO+1 (for the *E* isomer). The lower HOMO–LUMO energy gap of the *E* isomer compared to its *Z* counterpart (Fig. 6), comports with its additionally red-shifted absorption profile (Fig. 7a). This study further clarifies that the introduction of the electron-donating methoxy (–OMe) group in **(±)-3-*Z*** promotes a bathochromic shift in the absorption profile compared to compound **(±)-2-*Z***, due to a decrease in the HOMO–LUMO energy gap (Tables S2 and S3).

Due to the excellent solubility of compound **(±)-1-*Z***, we were able to measure its absorption spectrum in different polarity solvents (Fig. S78b). An almost identical absorption maximum is observed in non-polar solvents like methylcyclohexane (λ_{max} = 414 nm) and toluene (λ_{max} = 417 nm), as compared to moderately polar chloroform (λ_{max} = 416 nm). However, a 14 nm blue-shift is observed in a more polar solvent like acetonitrile (λ_{max} = 404 nm). Similarly, for compounds **(±)-2-*Z*** and **(±)-3-*Z***, a hypsochromic shift is observed in acetonitrile compared to chloroform and toluene (Fig. S79). Interestingly, the primary absorption bands are structured in non-polar media, unlike in the polar ones, possibly due to different solute–solvent interactions. This phenomenon, along with the hypsochromic shift in more polar media, is well-understood in push–pull type oligomers.[79,80] We also have observed evidence of possible π–π interactions in solution, as reported by a variable temperature (VT) UV–vis study (20 μM, tetrachloroethane) of compound **(±)-3-*Z*** (Fig. S86a). Upon increasing the temperature from 25 °C to 90 °C, a characteristic blue-shift ($\Delta\lambda_{max}$ = 7 nm) is observed, along with a decrease in the molar absorptivity. The

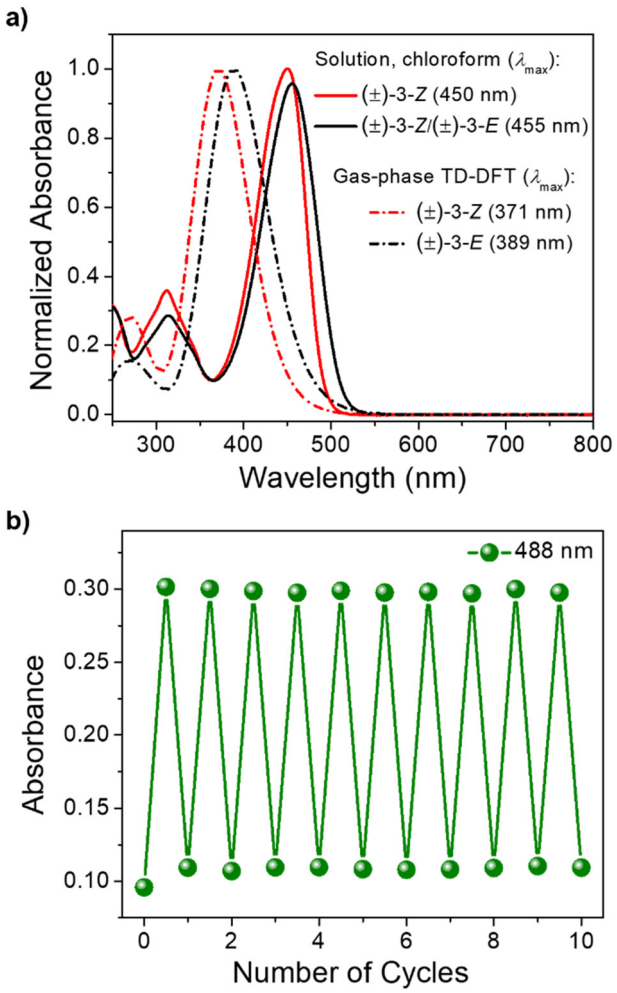

Fig. 7 (a) Experimental (solid lines) UV–vis (20 μM, chloroform) profiles of pure (±)-3-*Z* (red spectrum) and a (±)-3-*Z*/(±)-3-*E* mixture obtained upon 404 nm photoirradiation (black spectrum); and gas phase TD-DFT-predicted (dashed lines) absorption profiles of compounds (±)-3-*Z* (red spectrum) and (±)-3-*E* (black spectrum). (b) UV–vis photoswitching of compound (±)-3-*Z* (20 μM, chloroform). The absorbance change at 488 nm was monitored while alternating between 404 and 523 nm irradiation.

reversible change in the absorption profile (Fig. 86b) in addition to the VT NMR findings (Fig. S76 and S77), possibly correspond to the formation of π-stacked dimers in solution consistent with the solid-state X-ray crystallographic results (Fig. 3c).[81]

The *Z*/*E* photoisomerization was assessed in four different solvents for compound (±)-1-*Z* using selective excitation at 371, 404, and 454 nm (Fig. S82 and S83). As monitored by UV-vis spectroscopy, the $Z \rightarrow E$ isomerization follows a very similar trend in all the solvents and is consistent with the NMR results. There is a noticeable decrease in the molar absorptivity of the primary (λ = ~410 nm) and secondary (λ = ~300 nm) absorption bands, accompanied by a slight red shift of the absorption of the (±)-1-*Z*/(±)-1-*E* mixture compared to pure (±)-1-*Z*, as obtained upon photoirradiation at the PSS. Well-controlled $Z \rightarrow E$ photoisomerization (20 μM, chloroform) is observed for compounds (±)-2 (Fig. S84a) and (±)-3 (Fig. 7a and S84b) upon 371, 404, and 454 nm selective irradiation, which follows a similar trend in the UV-vis profiles for the *Z*/*E* mixture as compound (±)-1. The isomerization details observed from UV–vis studies are in good agreement with the NMR data.

The excited-state TD-DFT calculations reveal that the absorption maximum (calculated in the gas-phase) of 2-*Z*-C_A is 357 nm, while the maximum for 2-*E*-C_A is at 375 nm (Fig. S80a). The red-shifted absorption profiles (λ_{max} = 373 nm for 2-*Z*-C_A and 389 nm for 2-*E*-C_A) observed using the IEFPCM solvent model (Fig. S80b) are expected given the change in the dielectric properties offered by the solvent *versus* the in-vacuum conditions for the gas phase calculations.[82]

The 3-*E*-C_A isomer boasts a more red-shifted absorption maximum (λ_{max} = 389 nm) than 3-*Z*-C_A (λ_{max} = 371 nm). This TD-DFT predicted trend ($\Delta\lambda_{max}$ = 18 nm; Fig. 7a, dashed lines) matches perfectly with the experimentally observed UV-vis profiles ($\Delta\lambda_{max}$ = 5 nm; Fig. 7a, solid lines). To be noted, the difference between the *Z*/*E* absorption profiles ($\Delta\lambda_{max}$ = 18 nm) remains constant even upon tuning the electronics of the pCp core, and the small difference in the absorption spectra of *Z* and *E* isomers could explain the incomplete photoisomerization for these compounds. However, the electron-donating substituents could influence the mechanism of isomerization,[76,83] and this will be considered in future investigations.

The TD-DFT predicted UV-vis profiles as calculated for both compounds (±)-2 and (±)-3 in the C_B are summarized in the SI (Fig. S80, S81 and Tables S2, S3). Overall, the theoretical investigation provides an in-depth understanding of the RCN-decorated pCp molecules and aligns well with the experimental findings.

We evaluated the reversibility of the *Z*/*E* photoisomerization reactions by performing photoswitching studies with compound (±)-3-*Z* using alternating 404 and 523 nm irradiation (Fig. 7b). Compound (±)-3-*Z* was irradiated in solution (20 μM, chloroform) with a shorter wavelength light source (λ_{irr} = 404 nm) to promote $Z \rightarrow E$ isomerization to obtain a PSS, while exposing the PSS mixture to a longer wavelength of irradiation (λ_{irr} = 523 nm) promoted $E \rightarrow Z$ isomerization until a new PSS was reached. Excitingly, even after ten photoswitching cycles, almost no evidence of photodegradation was observed (Fig. 7b). This excellent fatigue-resistant and facile photoswitching performance using visible light excitation bodes well for designing photoresponsive materials.

While the well-behaved photoisomerization in different solvents and excellent photostability of these [2.2]pCp-based analogs are encouraging, the strong absorbance in the visible region for these systems might be attractive for optoelectronic applications.

Synthesis of an enantioenriched chiral photoswitch

Following the well-behaved photoisomerization behavior of the racemic chiral conjugated molecules, we were prompted to synthesize a representative enantioenriched RCN–pCp conjugate to evaluate its chiroptical properties. The synthesis of photo-

switch (R_p)-2-*Z* starts from the *racemic*-4-formyl-[2.2]paracyclophane ((±)-**5**). The aldehyde was reacted with (*S*)-(−)-α-phenylethylamine to form a mixture of imine diastereomers, which, after three rounds of recrystallization, yielded diastereopure (S,R_p)-**10**. The imine was subsequently hydrolyzed to enantioenriched aldehyde (R_p)-**5** (ee = 82%) using a silica plug (Schemes 2 and S4).[84] Finally, (R_p)-**5** was condensed with the RCN unit **6** to synthesize enantioenriched (ee = 90%) chiral photoswitch (R_p)-2-*Z* (Scheme 2). The optical purities of compounds (R_p)-**5** and (R_p)-2-*Z* were determined by High-Performance Liquid Chromatography (HPLC) using a chiral column (Fig. S49–S52). The detailed spectroscopic characterization of the resolved intermediates and compound (R_p)-2-*Z* is available in the SI (Fig. S11–S14 and S25, S26).

Reversible photoisomerization and chiroptical properties

The *Z*/*E* photoisomerization of the enantioenriched (R_p)-2-*Z* was monitored using NMR (15 mM, chloroform-*d*) and UV-vis (20 μM, chloroform). The PSDs ((R_p)-2-*Z*/(R_p)-2-*E*) emerge as 43/57 ($Z \rightarrow E$, λ_{irr} = 404 nm) and 92/8 ($E \rightarrow Z$, λ_{irr} = 454 nm) from the NMR studies (Fig. S63). A gradual decrease in absorbance is observed (λ_{irr} = 404 nm), accompanied by a slight red shift upon $Z \rightarrow E$ photoisomerization (Fig. 8a and S85). A very similar extent of isomerization was observed for the enantioenriched molecule compared to its racemic analog, suggesting no influence of the optical purity of these planar chiral molecules on their photoisomerization behavior.

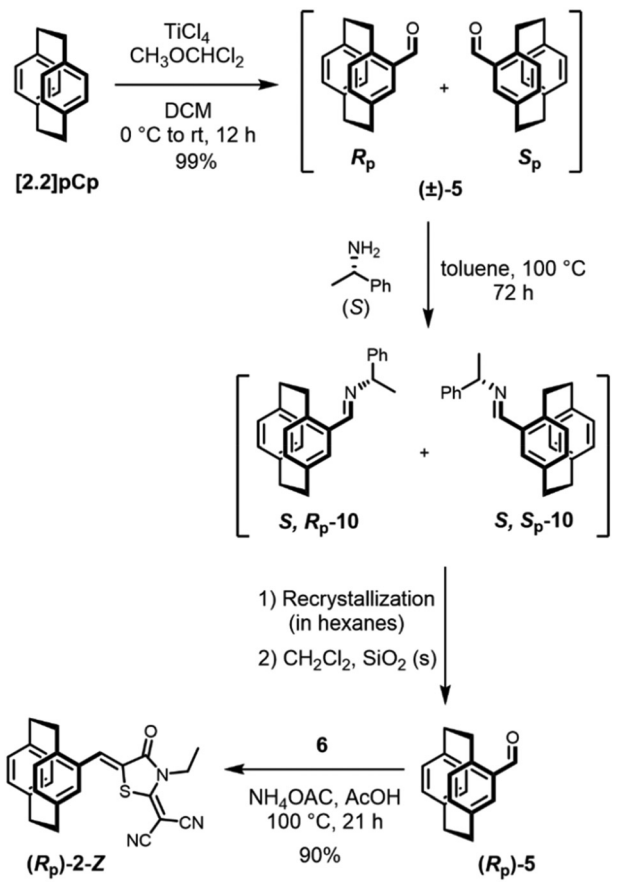

Scheme 2 Synthesis of the enantioenriched target molecule (R_p)-2-*Z*.

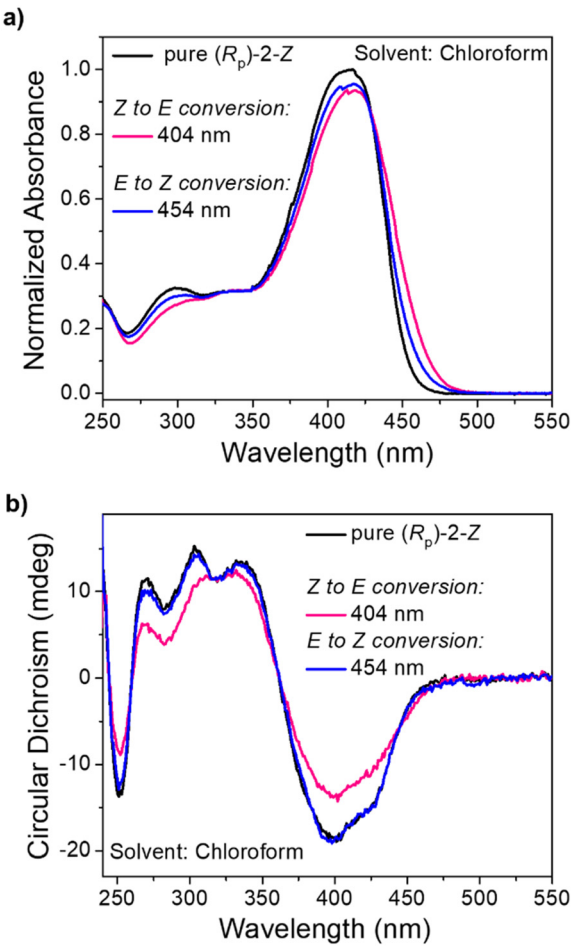

Fig. 8 Solution (20 μM, chloroform) (a) UV–vis and (b) circular dichroism (CD) profiles of pure (R_p)-2-*Z* (black trace) and the (R_p)-2-*Z*/(R_p)-2-*E* mixture obtained upon 404 nm irradiation ($Z \rightarrow E$ isomerization, pink trace) and 454 nm irradiation ($E \rightarrow Z$ isomerization, blue trace).

Inspired by the chiroptical properties of [2.2]pCp scaffolds,[85,86] we measured the electronic circular dichroism (ECD) spectrum of the planar chiral enantioenriched (R_p)-2-*Z* (20 μM, chloroform) and monitored the change upon *Z*/*E* photoisomerization (Fig. 8b). For the pure *Z* isomer, a negative response is observed at 401 nm ($\Delta\varepsilon$ = −19 M^{-1} cm^{-1}) along with a shoulder at 430 nm ($\Delta\varepsilon$ = −13 M^{-1} cm^{-1}). In the shorter wavelength region, several positive ECD-active bands are observed at 270 nm ($\Delta\varepsilon$ = +6 M^{-1} cm^{-1}) and 305–330 nm ($\Delta\varepsilon$ = +12 M^{-1} cm^{-1}). Upon $Z \rightarrow E$ isomerization promoted by 404 nm irradiation, a distinct spectral change is observed (Fig. 8b). The intensity of the band at 401 nm weakened ($\Delta\varepsilon$ = −13 M^{-1} cm^{-1}), while that of the positive bands at 270 nm, 304 nm, and 335 nm also decreased. Interestingly, by switching the irradiation source to 454 nm ($E \rightarrow Z$ isomerization), the ECD spectrum of the pure *Z* could be restored.

The magnitude of the change in chiroptical response is not large, which could be attributed to the incomplete photoisome-

rization of the RCN–pCp molecule, and the large overlap of the *Z* and *E* absorption profiles. We envision that tuning the isomer structures with substantial spectral separation and quantitative isomerization could facilitate more pronounced chiroptical changes, a concept currently being investigated in our group using the RCN–pCp scaffolds. However, considering the diverse applications of the [2.2]pCp-based π-conjugated moieties in supramolecular chemistry and organic materials, this light-modulated reversible chiroptical property of the reported RCN–pCp conjugates is exciting and would accentuate this scaffold as a promising candidate for future applications.

The experimental CD profiles are supported by TD-DFT calculations (at the B3LYP/6-31+G(d) level of theory). A negative response at 437 nm is obtained ($\Delta\varepsilon$ = −23 M^{-1} cm^{-1}) for the *Z* isomer (Fig. S88), which for the *E* isomer is observed at 457 nm ($\Delta\varepsilon$ = −19 M^{-1} cm^{-1}). Similar to the solution spectra, the positive bands in the lower wavelength regions are less intense for the *E* isomer compared to the *Z*. The consistency of the calculated and experimental ECD characteristics confirm that the reversibility observed in solution is only due to the *Z*/*E* photoisomerization process.

Thermal isomerization studies

We investigated whether the metastable *E* isomer can thermally relax back to the *Z* isomer in solution by ^{1}H NMR spectroscopy. Compound **(±)-1-*Z*** was first irradiated (λ_{irr} = 404 nm) to reach a PSS **(±)-1-*Z***/**(±)-1-*E*** mixture in three different solvents (toluene-d_8, chloroform-*d*, and acetonitrile-d_3). No noticeable *E* → *Z* thermal isomerization was observed within 24 h at 25 °C (Fig. S67–S69). As our previous work showed that RCN-based small-molecules[56] and related donor–acceptor-like structures[87] undergo faster thermal isomerization in more polar media, we tested the thermal stability of the pCp structures (**(±)-1-*Z***–**(±)-3-*Z***) in acetonitrile at 60 °C over 5 days (Fig. S70–S74). Monitoring the *Z*/*E* PSS mixtures for compounds **(±)-1-*Z*** (Fig. S70) and **(±)-2-*Z*** (Fig. S72), a thermal conversion (*E* → *Z*) of 16% and 9.1% was achieved. Compound **(±)-3-*Z*** (Fig. S74) undergoes the highest extent (28%) of thermal relaxation (*E* → *Z*) under the same experimental conditions, which highlights that the electron-donating influence of the methoxy substituent could accelerate the olefin isomerization thermally (Fig. S75).[88] We have shown that even minor molecular engineering can impact the thermal stability of these molecules.

Conclusions

We have designed and synthesized novel planar chiral photoswitches based on [2.2]pCp–RCN conjugates. The as-synthesized isomer exists in the *Z* configuration about the exocyclic olefin bond, as confirmed by X-ray crystallography and comprehensive 2D-NMR spectroscopic studies. These conjugated small molecules can undergo reversible *Z*/*E* photoisomerization using visible and UV light irradiation efficiently. A PSD of 40/60 (*Z*/*E*) was obtained for compound **(±)-3-*Z*** upon *Z* → *E* isomerization, while near quantitative (98%) *E* → *Z* conversion was achieved. The NMR and UV–vis isomerization results are complementary, with the UV-vis profiles showing negative solvatochromism for compound **(±)-1-*Z*** in different polarity solvents (methylcyclohexane, toluene, chloroform, and acetonitrile). Introduction of an electron-donating methoxy (–OMe) group red shifts the absorption of **(±)-3-*Z*** to 450 nm and promotes excellent photoswitching performance upon alternating 404 and 523 nm irradiation. The metastable *E* isomer could be purified (up to 94%) and structurally characterized. Detailed DFT and TD-DFT calculations correlate well with the experimental outcomes; a very similar trend in UV–vis profiles is obtained for the *Z* and *E* isomers in solution (chloroform) and gas-phase calculations. In-depth inspection of the frontier molecular orbitals also provides insight into the spectroscopic transition.

Most interestingly, synthesis and characterization of enantioenriched RCN-pCp **(R_p)-2-*Z*** has revealed that the characteristic CD signal of the *Z* isomer could be modulated with 404 nm irradiation, owing to *Z* → *E* isomerization, and restored with exposure to a 454 nm LED (*E* → *Z* isomerization). Simulated CD profiles from TD-DFT calculations also corroborate these findings. Reversible control of the optical and chiroptical properties is highly encouraging and holds potential for designing photoresponsive functional materials in the future. Overall, this work presents the [2.2]pCp–RCN conjugates as novel planar chiral molecular photoswitches with reversible chiroptical properties. Further molecular engineering to develop high-performing chiroptical switches based on this chiral RCN–pCp structure is underway in our group.

Author contributions

P. Das, C. D. Stearns, and R. K. Castellano conceived the project. P. Das and C. D. Stearns performed the syntheses. P. Das conducted the photophysical and photoisomerization experiments. I. Ghiviriga performed the 2D NMR experiments, and Ł. Dobrzycki performed the X-ray crystal analyses. R. K. Castellano supervised the project. All of the authors contributed to the manuscript writing and have given approval to the final version of the manuscript.

Conflicts of interest

There are no conflicts to declare.

Data availability

The data supporting this article have been included as part of the supplementary information (SI). Synthesis schemes, witten characterization data, 1D and 2D NMR spectra, HPLC details, NMR and UV-vis solution photoisomerization and thermal isomerization studies, and X-ray crystallography details are included in the SI. Supplementary information is available. See DOI: **https://doi.org/10.1039/d5qo01401h**.

CCDC 2480804 contains the supplementary crystallographic data for this paper.[89]

Acknowledgements

We are grateful to the National Science Foundation (NSF) for funding this research (NSF, CHE-2203754). We acknowledge the University of Florida Research Computing for providing computational resources and support that have contributed to the research results reported in this publication (**https://www.rc.ufl.edu**). RKC is grateful to Steven M. and Rebecca J. Scott for providing the endowment that funded a portion of this research. The mass spectrometric data were obtained by the UF Department of Chemistry Mass Spectrometry Research and Education Center, supported in part by the National Institutes of Health (NIH S10 OD021758-01A1 and S10 OD030250-01A1). We would like to thank the UF Center for Nuclear Magnetic Resonance Spectroscopy for providing equipment and support that have contributed to these published results. The X-ray measurement was performed at the Center for X-ray Crystallography in the Department of Chemistry at the University of Florida. The NSF (CHE-1828064) and UF are greatly acknowledged for funding the X-ray diffractometer. Acknowledgement is made to Divya Radhakrishnan (University of Florida) for technical assistance with the HPLC analyses and Cory Kornman (University of Florida) for the synthesis of one precursor molecule.

References

1 B. L. Feringa, R. A. Van Delden, N. Koumura and E. M. Geertsema, Chiroptical Molecular Switches, *Chem. Rev.*, 2000, **100**, 1789–1816.
2 B. L. Feringa, The Art of Building Small: From Molecular Switches to Molecular Motors, *J. Org. Chem.*, 2007, **72**, 6635–6652.
3 D. Sahoo, R. Benny, N. K. Ks and S. De, Stimuli-Responsive Chiroptical Switching, *ChemPlusChem*, 2022, **87**, e202100322.
4 Z. Dai, J. Lee and W. Zhang, Chiroptical Switches: Applications in Sensing and Catalysis, *Molecules*, 2012, **17**, 1247–1277.
5 B. L. Feringa and R. A. van Delden, Absolute Asymmetric Synthesis: The Origin, Control, and Amplification of Chirality, *Angew. Chem., Int. Ed.*, 1999, **38**, 3418–3438.
6 H. K. Bisoyi and Q. Li, Light-Driven Liquid Crystalline Materials: From Photo-Induced Phase Transitions and Property Modulations to Applications, *Chem. Rev.*, 2016, **116**, 15089–15166.
7 Y. Wang and Q. Li, Light-Driven Chiral Molecular Switches or Motors in Liquid Crystals, *Adv. Mater.*, 2012, **24**, 1926–1945.
8 M. L. C. M. Oosterling, A. M. Schoevaars, H. J. Haitjema and B. L. Feringa, Polymer-Bound Chiroptical Molecular Switches; Photochemical Modification of the Chirality of Thin Films, *Isr. J. Chem.*, 1996, **36**, 341–348.
9 L. Zhang, H.-X. Wang, S. Li and M. Liu, Supramolecular chiroptical switches, *Chem. Soc. Rev.*, 2020, **49**, 9095–9120.
10 F. Xu and B. L. Feringa, Photoresponsive supramolecular polymers: from light–controlled small molecules to smart materials, *Adv. Mater.*, 2023, **35**, 2204413.
11 Y. Qiu, P. Chen, P. Guo, Y. Li and M. Liu, Supramolecular Chiroptical Switches Based on Achiral Molecules, *Adv. Mater.*, 2008, **20**, 2908–2913.
12 Y. Hashimoto, T. Nakashima, M. Yamada, J. Yuasa, G. Rapenne and T. Kawai, Hierarchical Emergence and Dynamic Control of Chirality in a Photoresponsive Dinuclear Complex, *J. Phys. Chem. Lett.*, 2018, **9**, 2151–2157.
13 Y. Hashimoto, T. Nakashima, D. Shimizu and T. Kawai, Photoswitching of an intramolecular chiral stack in a helical tetrathiazole, *Chem. Commun.*, 2016, **52**, 5171–5174.
14 Y. Xie, D. Fu, O. Jin, H. Zhang, J. Wei and J. Guo, Photoswitchable molecular switches featuring both axial and tetrahedral chirality, *J. Mater. Chem. C*, 2013, **1**, 7346–7356.
15 S. Wiedbrauk and H. Dube, Hemithioindigo—an emerging photoswitch, *Tetrahedron Lett.*, 2015, **56**, 4266–4274.
16 J. E. Zweig and T. R. Newhouse, Isomer-Specific Hydrogen Bonding as a Design Principle for Bidirectionally Quantitative and Redshifted Hemithioindigo Photoswitches, *J. Am. Chem. Soc.*, 2017, **139**, 10956–10959.
17 B. Shao and I. Aprahamian, Hydrazones as New Molecular Tools, *Chem*, 2020, **6**, 2162–2173.
18 B. Balamut and I. Aprahamian, Molecular Steganography Using Multistate Photoswitchable Hydrazones, *J. Am. Chem. Soc.*, 2025, **147**, 19444–19449.
19 S. Adak, I. Ghosh, M. L. Maity and S. Bandyopadhyay, Arylazopyrazole Photoconversion Enables Tunable Morphology and Mechanical Properties, *Small*, 2025, **21**, 2412482.
20 N. Nogal, S. Guisán, D. Dellemme, M. Surin and A. de la Escosura, Selectivity in the chiral self-assembly of nucleobase-arylazopyrazole photoswitches along DNA templates, *J. Mater. Chem. B*, 2024, **12**, 3703–3709.
21 B. Shao, H. Fu and I. Aprahamian, A molecular anion pump, *Science*, 2024, **385**, 544–549.
22 Q. Qi, Y. Liu, V. Puranik, S. Patra, Z. Svindrych, X. Gong, Z. She, Y. Zhang and I. Aprahamian, Photoswitchable Fluorescent Hydrazone for Super-Resolution Cell Membrane Imaging, *J. Am. Chem. Soc.*, 2025, **147**, 16404–16411.
23 J. Boelke and S. Hecht, Designing Molecular Photoswitches for Soft Materials Applications, *Adv. Opt. Mater.*, 2019, **7**, 1900404.
24 C. Petermayer and H. Dube, Circular Dichroism Photoswitching with a Twist: Axially Chiral Hemiindigo, *J. Am. Chem. Soc.*, 2018, **140**, 13558–13561.
25 F. Kohl, T. Vogl, F. Hampel and H. Dube, Hemiphosphoindigos as a Platform for Chiroptical or Water Soluble Photoswitching, *Nat. Commun.*, 2025, **16**, 1760.
26 T. J. Wigglesworth, D. Sud, T. B. Norsten, V. S. Lekhi and N. R. Branda, Chiral Discrimination in Photochromic Helicenes, *J. Am. Chem. Soc.*, 2005, **127**, 7272–7273.

27 T. Nakagawa, R. Kato, Y. Iiyoshi, M. Furuya, T. Kitano, R. Nakamura, Y. Yokoyama and T. Ubukata, A chiral photoswitch based on enantiospecific interconversion between binaphthyl and helicenoid skeletons, *Chem. Commun.*, 2024, **60**, 5149–5152.
28 B. L. Feringa, W. F. Jager, B. De Lange and E. W. Meijer, Chiroptical molecular switch, *J. Am. Chem. Soc.*, 1991, **113**, 5468–5470.
29 R. A. van Delden, M. B. van Gelder, N. P. M. Huck and B. L. Feringa, Controlling the Color of Cholesteric Liquid-Crystalline Films by Photoirradiation of a Chiroptical Molecular Switch Used as Dopant, *Adv. Funct. Mater.*, 2003, **13**, 319–324.
30 E. D. King, P. Tao, T. T. Sanan, C. M. Hadad and J. R. Parquette, Photomodulated Chiral Induction in Helical Azobenzene Oligomers, *Org. Lett.*, 2008, **10**, 1671–1674.
31 K. Rijeesh, P. K. Hashim, S.-i. Noro and N. Tamaoki, Dynamic induction of enantiomeric excess from a prochiral azobenzene dimer under circularly polarized light, *Chem. Sci.*, 2015, **6**, 973–980.
32 C. Brown and A. Farthing, Preparation and structure of di-p-xylylene, *Nature*, 1949, **164**, 915–916.
33 D. J. Cram and H. Steinberg, Preparation and spectra of the paracyclophanes, *J. Am. Chem. Soc.*, 1951, **73**, 5691–5704.
34 H. Hope, J. Bernstein and K. Trueblood, The crystal and molecular structure of 1, 1, 2, 2, 9, 9, 10, 10-octafluoro-[2, 2] paracyclophane and a reinvestigation of the structure of [2, 2] paracyclophane, *Struct. Sci.*, 1972, **28**, 1733–1743.
35 D. J. Cram, N. L. Allinger and H. Steinberg, The Spectral Consequences of Bringing Two Benzene Rings Face to Face, *J. Am. Chem. Soc.*, 1954, **76**, 6132–6141.
36 D. E. Fagnani, M. J. Meese Jr, K. A. Abboud and R. K. Castellano, Homochiral [2.2]Paracyclophane Self-Assembly Promoted by Transannular Hydrogen Bonding, *Angew. Chem., Int. Ed.*, 2016, **55**, 10726–10731.
37 C. D. Stearns, A. Kumar, I. Ghiviriga, L. M. Dobrzycki, K. A. Abboud and R. K. Castellano, Mixed Amide Paracyclophane Assemblies Emulating Supramolecular Copolymers, *J. Am. Chem. Soc.*, 2025, **147**, 24615–24627.
38 W. Liu, H. Li, Y. Huo, Q. Yao and W. Duan, Recent Progress in Research on [2.2]Paracyclophane-Based Dyes, *Molecules*, 2023, **28**, 2891.
39 Z. Hassan, Molecular Insights into [2.2]Paracyclophane-Based Functional Materials: Chemical Aspects Behind Functions, *Adv. Funct. Mater.*, 2024, **34**, 2311828.
40 D. J. Cram and N. L. Allinger, Stereochemical Consequences of Steric Compression in the Smallest Paracyclophane, *J. Am. Chem. Soc.*, 1955, **77**, 6289–6294.
41 M. Gon, Y. Morisaki and Y. Chujo, Optically active cyclic compounds based on planar chiral [2.2] paracyclophane: extension of the conjugated systems and chiroptical properties, *J. Mater. Chem. C*, 2015, **3**, 521–529.
42 G. P. Bartholomew, M. Rumi, S. J. Pond, J. W. Perry, S. Tretiak and G. C. Bazan, Two-photon absorption in three-dimensional chromophores based on [2.2]-paracyclophane, *J. Am. Chem. Soc.*, 2004, **126**, 11529–11542.
43 Y. Yang, G. Zhang, C. Yu, C. He, J. Wang, X. Chen, J. Yao, Z. Liu and D. Zhang, New conjugated molecular scaffolds based on [2, 2] paracyclophane as electron acceptors for organic photovoltaic cells, *Chem. Commun.*, 2014, **50**, 9939–9942.
44 G. Albano, G. Pescitelli and L. Di Bari, Chiroptical Properties in Thin Films of π-Conjugated Systems, *Chem. Rev.*, 2020, **120**, 10145–10243.
45 Z. Hassan, Molecular Insights into [2.2] Paracyclophane–Based Functional Materials: Chemical Aspects Behind Functions, *Adv. Funct. Mater.*, 2024, **34**, 2311828.
46 P. K. Hashim, M. C. Basheer and N. Tamaoki, Chirality induction by E–Z photoisomerization in [2,2]paracyclophane-bridged azobenzene dimer, *Tetrahedron Lett.*, 2013, **54**, 176–178.
47 K. Mutoh, M. Sliwa and J. Abe, Rapid Fluorescence Switching by Using a Fast Photochromic [2.2] Paracyclophane-Bridged Imidazole Dimer, *J. Phys. Chem. C*, 2013, **117**, 4808–4814.
48 R. Reuter and H. A. Wegner, Oligoazobenzenophanes—synthesis, photochemistry and properties, *Chem. Commun.*, 2011, **47**, 12267–12276.
49 G. Ouyang, D. Bialas and F. Würthner, Reversible fluorescence modulation through the photoisomerization of an azobenzene-bridged perylene bisimide cyclophane, *Org. Chem. Front.*, 2021, **8**, 1424–1430.
50 J. Lu, W. Gu, J. Wei, W. Zhang, Z. Zhang, Y. Yu, N. Zhou and X. Zhu, Novel planar chiral dopants with high helical twisting power and structure-dependent functions, *J. Mater. Chem. C*, 2016, **4**, 9576–9580.
51 M. Mathews and N. Tamaoki, Planar Chiral Azobenzenophanes as Chiroptic Switches for Photon Mode Reversible Reflection Color Control in Induced Chiral Nematic Liquid Crystals, *J. Am. Chem. Soc.*, 2008, **130**, 11409–11416.
52 A. Insuasty, A. Ortiz, A. Tigreros, E. Solarte, B. Insuasty and N. Martín, 2-(1, 1-dicyanomethylene) rhodanine: A novel, efficient electron acceptor, *Dyes Pigm.*, 2011, **88**, 385–390.
53 B. Kan, M. Li, Q. Zhang, F. Liu, X. Wan, Y. Wang, W. Ni, G. Long, X. Yang, H. Feng, Y. Zuo, M. Zhang, F. Huang, Y. Cao, T. P. Russell and Y. Chen, A Series of Simple Oligomer-like Small Molecules Based on Oligothiophenes for Solution-Processed Solar Cells with High Efficiency, *J. Am. Chem. Soc.*, 2015, **137**, 3886–3893.
54 C. T. Kornman, L. Li, A. O. Weldeab, I. Ghiviriga, K. A. Abboud and R. K. Castellano, Photoisomerization of dicyanorhodanine-functionalized thiophenes, *Chem. Sci.*, 2020, **11**, 10190–10197.
55 P. Das, N. J. Grinalds, I. Ghiviriga, K. A. Abboud, Ł. Dobrzycki, J. Xue and R. K. Castellano, Dicyanorhodanine-Pyrrole Conjugates for Visible Light-Driven Quantitative Photoswitching in Solution and the Solid State, *J. Am. Chem. Soc.*, 2024, **146**, 11932–11943.
56 C. T. Kornman, P. Das, L. Li, A. O. Weldeab, I. Ghiviriga and R. K. Castellano, 2-(1,1-Dicyanomethylene)rhodanine-Functionalized Oligothiophenes: A Structure–Property

Investigation of Z/E Photoisomerization Behavior, *J. Org. Chem.*, 2024, **89**, 13853–13867.

57 D. M. Camero, N. J. Grinalds, C. T. Kornman, S. Barba, L. Li, A. O. Weldeab, R. K. Castellano and J. Xue, Thin-Film Morphology and Optical Properties of Photoisomerizable Donor–Acceptor Oligothiophenes, *ACS Appl. Mater. Interfaces*, 2023, **15**, 25134–25147.

58 D. S. Seferos, A. S. Blum, J. G. Kushmerick and G. C. Bazan, Single-Molecule Charge-Transport Measurements that Reveal Technique-Dependent Perturbations, *J. Am. Chem. Soc.*, 2006, **128**, 11260–11267.

59 D. S. Seferos, S. A. Trammell, G. C. Bazan and J. G. Kushmerick, Probing π-coupling in molecular junctions, *Proc. Natl. Acad. Sci. U. S. A.*, 2005, **102**, 8821–8825.

60 T. Sato and K. Torizuka, Structure and anodic peak potential relationships. Cyclophanes. Cyclic voltammetric studies of cation-radical formation and reactions, *J. Chem. Soc., Perkin Trans. 2*, 1978, 1199–1204.

61 T. Sato, K. Torizuka, R. Komaki and H. Atobe, Transannular interaction and reactions of 5,13-disubstituted [2.2]metacyclophanes: substituent effects on carbon-13 n.m.r. spectra, cyclic voltammetric peak potentials, and anodic oxidation, *J. Chem. Soc., Perkin Trans. 2*, 1980, 561–568.

62 S. Canuto and M. C. Zerner, Theoretical interpretation of the absorption and ionization spectra of the paracyclophanes, *J. Am. Chem. Soc.*, 1990, **112**, 2114–2120.

63 M. V. Ivonina, Y. Orimoto and Y. Aoki, Quantum chemistry–machine learning approach for predicting and elucidating molecular hyperpolarizability: Application to [2.2]paracyclophane-containing push–pull polymers, *J. Chem. Phys.*, 2021, **154**, 124107.

64 A. de la Escosura, C. G. Claessens, I. Ledoux-Rak, J. Zyss, M. V. Martínez-Díaz and T. Torres, [2,2]paracyclophane-bisphthalocyanines: non-classical push-pull systems for second harmonic generation, *J. Porphyrins Phthalocyanines*, 2005, **09**, 788–793.

65 M. V. Ivonina, Y. Orimoto and Y. Aoki, Nonlinear optical properties of push-pull systems containing [2.2]paracyclophane: Theoretical study via elongation method, *Chem. Phys. Lett.*, 2020, **755**, 137760.

66 F. Aleotti, A. Nenov, L. Salvigni, M. Bonfanti, M. M. El-Tahawy, A. Giunchi, M. Gentile, C. Spallacci, A. Ventimiglia, G. Cirillo, L. Montali, S. Scurti, M. Garavelli and I. Conti, Spectral Tuning and Photoisomerization Efficiency in Push–Pull Azobenzenes: Designing Principles, *J. Phys. Chem. A*, 2020, **124**, 9513–9523.

67 M. Zitzmann, M. Fröhling and H. Dube, Gain of Function Recyclable Photoswitches: Reversible Simultaneous Substitution and Photochromism Generation, *Angew. Chem., Int. Ed.*, 2024, **63**, e202318767.

68 H. Hu, B. Liu, M. Li, Z. Zheng and W.-H. Zhu, A Quadri-Dimensional Manipulable Laser with an Intrinsic Chiral Photoswitch, *Adv. Mater.*, 2022, **34**, 2110170.

69 Z. Zheng, H. Hu, Z. Zhang, B. Liu, M. Li, D.-H. Qu, H. Tian, W.-H. Zhu and B. L. Feringa, Digital photoprogramming of liquid-crystal superstructures featuring intrinsic chiral photoswitches, *Nat. Photonics*, 2022, **16**, 226–234.

70 H. Liu, W. Wang, Y. Zhou and Z. a. Li, A ring-locking strategy to enhance the chemical and photochemical stability of A–D–A-type non-fullerene acceptors, *J. Mater. Chem. A*, 2021, **9**, 1080–1088.

71 C. J. Friedmann, S. Ay and S. Bräse, Improved Synthesis of Enantiopure 4-Hydroxy[2.2]paracyclophane, *J. Org. Chem.*, 2010, **75**, 4612–4614.

72 E. V. Sergeeva, V. I. Rozenberg, D. Y. Antonov, E. V. Vorontsov, Z. A. Starikova, I. V. Fedyanin and H. Hopf, Novel Multichiral Diols and Diamines by Highly Stereoselective Pinacol Coupling of Planar Chiral [2.2]Paracyclophane Derivatives, *Chem. – Eur. J.*, 2005, **11**, 6944–6961.

73 S. Miertuš, E. Scrocco and J. Tomasi, Electrostatic interaction of a solute with a continuum. A direct utilizaion of AB initio molecular potentials for the prevision of solvent effects, *Chem. Phys.*, 1981, **55**, 117–129.

74 J. L. Pascual-ahuir, E. Silla and I. Tuñon, A new algorithm for the computation of a solvent-excluding surface, *J. Comput. Chem.*, 1994, **15**, 1127–1138.

75 S. Wiedbrauk, B. Maerz, E. Samoylova, A. Reiner, F. Trommer, P. Mayer, W. Zinth and H. Dube, Twisted Hemithioindigo Photoswitches: Solvent Polarity Determines the Type of Light-Induced Rotations, *J. Am. Chem. Soc.*, 2016, **138**, 12219–12227.

76 M. R. Lea, V. G. Stavros and R. J. Maurer, Effect of Electron Donating/Withdrawing Groups on Molecular Photoswitching of Functionalized Hemithioindigo Derivatives: a Computational Multireference Study, *ChemPhotoChem*, 2022, **6**, e202100290.

77 T. Cordes, T. Schadendorf, K. Rück-Braun and W. Zinth, Chemical control of Hemithioindigo-photoisomerization – Substituent-effects on different molecular parts, *Chem. Phys. Lett.*, 2008, **455**, 197–201.

78 A. Ali, M. I. Rafiq, Z. Zhang, J. Cao, R. Geng, B. Zhou and W. Tang, TD-DFT benchmark for UV-visible spectra of fused-ring electron acceptors using global and range-separated hybrids, *Phys. Chem. Chem. Phys.*, 2020, **22**, 7864–7874.

79 B. Carlotti, A. Cesaretti, C. G. Fortuna, A. Spalletti and F. Elisei, Experimental evidence of dual emission in a negatively solvatochromic push–pull pyridinium derivative, *Phys. Chem. Chem. Phys.*, 2015, **17**, 1877–1882.

80 A. Cesaretti, P. Foggi, C. G. Fortuna, F. Elisei, A. Spalletti and B. Carlotti, Uncovering Structure–Property Relationships in Push–Pull Chromophores: A Promising Route to Large Hyperpolarizability and Two-Photon Absorption, *J. Phys. Chem. C*, 2020, **124**, 15739–15748.

81 K. Ostrowska, D. Ceresoli, K. Stadnicka, M. Gryl, M. Cazzaniga, R. Soave, B. Musielak, Ł. J. Witek, P. Goszczycki and J. Grolik, π–π-Induced aggregation and single-crystal fluorescence anisotropy of 5, 6, 10b-triazaacephenanthrylene, *IUCrJ*, 2018, **5**, 335–347.

82 G. Scalmani, M. J. Frisch, B. Mennucci, J. Tomasi, R. Cammi and V. Barone, Geometries and properties of

excited states in the gas phase and in solution: Theory and application of a time-dependent density functional theory polarizable continuum model, *J. Chem. Phys.*, 2006, **124**, 094107.

83 B. Oruganti and B. Durbeej, On the possibility to accelerate the thermal isomerizations of overcrowded alkene-based rotary molecular motors with electron-donating or electron-withdrawing substituents, *J. Mol. Model*, 2016, **22**, 219.

84 E. Polat, O. Turbedaroglu and M. Cakici, Synthesis of bis (benzoxazole) frameworks chiralized by planar chiral [2.2] Paracyclophane, *Tetrahedron Lett.*, 2021, **67**, 152871.

85 M.-L. Delcourt, C. Reynaud, S. Turcaud, L. Favereau, J. Crassous, L. Micouin and E. Benedetti, 3D Coumarin Systems Based on [2.2]Paracyclophane: Synthesis, Spectroscopic Characterization, and Chiroptical Properties, *J. Org. Chem.*, 2019, **84**, 888–899.

86 S. Felder, M.-L. Delcourt, M. H. E. Bousquet, D. Jacquemin, R. Rodríguez, L. Favereau, J. Crassous, L. Micouin and E. Benedetti, Planar Chiral Analogues of PRODAN Based on a [2.2]Paracyclophane Scaffold: Synthesis and Photophysical Studies, *J. Org. Chem.*, 2022, **87**, 147–158.

87 P. Das, C. T. Kornman, I. Ghiviriga, K. A. Abboud and R. K. Castellano, Enlightening the Well-Controlled Photochemical Behavior of 1,1-Dicyanomethylene-3-Indanone-Functionalized π-Conjugated Molecules, *Chem. Mater.*, 2023, **35**, 8122–8134.

88 Y.-P. Wang, Z.-X. Zhang, M. Xie, F.-Q. Bai, P.-X. Wang and H.-X. Zhang, Theoretical study on thermal cis-to-trans isomerization of BF2-coordinated azo compounds of the para-substitution with electron donating groups, *Dyes Pigm.*, 2016, **129**, 100–108.

89 CCDC 2480804: Experimental Crystal Structure Determination, 2025, DOI: **10.5517/ccdc.csd.cc2p8gyd**.